PROCEEDINGS. "Twenty-Seventh Workshop on Geothermal Reservoir Engineering
Stanford University, Stanford, California, January 27-29, 2003

Decline Curve Analysis in a Naturally Fractured Reservoir with a Finite-Conductivity Fault

Héctor Pulido [1,2], Fernando Samaniego[2], Jesús Rivera[2] and Rodolfo Camacho [1,2]
1. Pemex, **2.** U. of México

Abstract

An analytical solution for constant producing pressure conditions for a well near a nonintersecting finite-conductivity fault, of infinite length in a naturally fractured reservoir, is presented. The solutions for the dimensionless flow rate are based on a model presented by Abaszadeh and Cinco-Ley. In this work the model was extended to include constant producing pressure in infinite systems. Flow along and across the fault plane is considered. It is demonstrated that a graph of q_D *vs* t_{Ddf} for long times produces a straight line with slope -1/4, it is proportional to $\sqrt{F_{CD}}$. Type curves in terms of fault conductivity and diffusivity ratios are presented. Finally, a field pressure-buildup test and production history data from a faulted reservoir that exhibit characteristics predicted by the analytical model are analyzed. The results show that the initial decline could be a key factor in deciding when to change or abandon a well, and for a practical viewpoint, given an initial value to the flow rate, it is important to know the time required to deplete the system composed by the naturally fractured reservoir and the finite conductivity fault.

Introduction

Due to tectonic related folding and displacements, the existence of faults in naturally fractured reservoirs (NFR's) is common, and often little information is available about their static and dynamic characteristics. Differentiating between sealing, partially sealing, and totally non sealing (transparent) faults to migration of fluids, is a major problem for geophysicists, geologists and reservoir engineers, working in reservoir characterization, geothermal and petroleum exploitation, development, and production[1]. Seismic attributes is a geophysical tool for detecting or looking for, the spatial orientation of the fault plane in the field; in addition different types of well logs are used for fault detection. Within the interpretation process of 3D seismic surveys, there are faults which can be defined by reprocessing data with refinated attributes. The dynamic characteristics of a fault can be obtained by either tracer tests or pressure transient analysis, including interference and pulse tests.

A *sealing fault* is often generated when the throw (vertical displacement of a dip-slip fault) of the fault plane is such that a permeable layer on one side of the fault plane is completely juxtaposed against an impermeable layer on the other side. It is also possible the precipitation and crystallization of minerals within the fault plane before oil migration into a reservoir.[2] In addition, a fluid carry out sediments and fines, and the fault can act as a filter and infill the fault plane.

A *nonsealing fault* usually has an insufficient throw to cause a complete separation of productive layers on the opposite sides of the fault plane. Because some mechanical and tectonic processes, such as folding, grain crushing, clay smearing, and possible geochemical alterations inside or around the fault, its permeability is different from the formation permeability. Depending on the permeability of the fault, fluid flow may occur along the fault within the fault plane, or just across it, laterally from one layer to another.

When a combined behavior of flow along and across the fault plane is present, it is known as a *finite-conductivity fault.* While sealing faults

block fluid and pressure communication with others regions of a reservoir, infinite-conductivity faults act as pressure support sources and allow fluid transfer across and along the fault planes. Finite conductivity faults are between these two limiting cases of sealing and totally transparent faults[1]. It has been shown that pressure-derivative type curves exhibit a quarter slope line bilinear flow behavior for high fault conductivities at long times, when the fault acts like a channel.

Pressure buildup and drawdown tests have been used to confirm the pressence of faults[3], as well as to obtain the distance and the dynamic characteristics of them. Knowledge of the static characterization or the geological model helps to select the adequate model.

The fault skin factor characterize flow across the fault, while its conductivity describes flow along the fault; zero conductivities represent *semipermeable faults* (leaky faults) However, a critical wellbore storage constant can also be identified above which the detection of the fault becomes impractical, and the quarter-slope straight-line pattern does not appear on pressure type curves due to the presence of a pseudoskin around the well.

Decline curve analysis offers a practical way to determine fluid *transmissibility* and *interconnectivity degree* of faults, using flow rate history data. Other information that can be obtained is the confirmation of the presence of different blocks sizes in the field.

Several models have been presented in the literature for fault characterization from pressure-transient tests. The simplest of such models uses the method of images for sealing faults, which rests in the identification of the pressence of a straight line, whose slope is double from the first one on a semilog plot of transient pressure tests.[4,6] Horner[3] investigated the presence of non-flow barriers based on the "double of slope rule" on a semilog plot of pressure buildup data. Davies and Hawkins[5] developed a method for estimation of the distance to linear barriers, based on the intersection of the two straight lines on a semilog plot. Earlougher and Kazemi[7] suggested the criteria for the required producing time to observe the double slope on the Horner plot. Field experience from reservoirs with fractures indicate that pressure responses usually exhibit transition periods, depicting the matrix pressure support of the fracture system.

Extensions to intersecting or nonintersecting multiple sealing faults have also been reported.[7-11] Cinco-Ley *et al.* [13] considered the finite conductivity-fault case and derived an analytical solution based on source functions.

The first attempt to represent a fault as a partial barrier was presented by Stewart *et al.;*[14] they numerically modeled the fault zone as a vertical semipermeable barrier of negligible capacity. This model correctly imposed the linear flow pattern at the fault plane. Yaxeley[15] derived analytical solutions for partially communicating faults, generalizing Bixel *et al*.[16] solution for reservoirs with a semi-impermeable linear discontinuity. Ambastha *et al*.[17] analytically modeled the partially communicating faults as presented by van Everdingen[18] and Hurst.[19]

The models considered by Stewart, Yaxely, and Ambastha allowed fluid transfer only laterally across the fault planes, but did not take into account fluid flow along the fault plane, which can occur when the permeability of the fault plane is larger than the reservoir permeability surrounding it. Khachatoorian et al.[20] developed an analytical model describing the pressure transient response in an NFR under the influence of a sealing fault; they found that a fault near the well affected the determination of the interporosity parameters.

Abbaszadeh and Cinco-Ley[21] presented a general analytical solution for the pressure-transient distribution in a reservoir, caused by an active well near a nonintersecting finite-conductivity fault. The model includes an alterated region around the fault zone, and allows for differing reservoir properties on either side of the fault plane, to more closely represent actual geological situations, when one stratum is juxtaposed against a different stratum. The solution considers flow both along and across the fault plane. Pressure derivatives exhibit a negative unit slope straight line, followed by quarter-slope bilinear flow characteristics for high-fault conductivities. They presented a method to calculate the

distance to conductive faults, based on a plot of pressure-derivative vs. reciprocal of shut-in time.

In addition, they presented type curves of pressure-drawdown behavior at an active well in terms of fault conductivity and skin factor.

Statement of Problem and Dimensionless Variables

Reservoir properties of the fault are considered to be different from those at the two sides of the fault plane; it would represent geological cases where one stratum is juxtaposed against another stratum with different properties.

The usual pressure-transient assumptions[22], such as isothermal flow, fluid with constant but small compressibility, and negligible gravitational effects, are also assumed.

Fig. 1 shows a visualization of a faulted reservoir.

Fig. 2 shows a schematic representation of a typical faulting system, along with the flow lines in the reservoir and within the fault plane.

Fig. 3 represents a simplification of the complex faulting configuration with the nomenclature for mathematical modeling purposes, shown in Fig. 3.

Dimensionless groups are defined as:

$$x_D = \frac{x}{d^2}; \qquad y_D = \frac{y}{d^2} \qquad ; r_{wD} = \frac{r_w}{d^2} \tag{1}$$

$$t_D = \frac{2.637\ x10^{-4}\, k_{fbi}\, t}{\left[\phi_{mbi} c_{tmbi} + \phi_{fbi} c_{tfbi}\right]\ \mu_i d^2}; \tag{2}$$

$$p_{fD}(r_D, t_D) = \frac{k_{fbi} h \quad [p_i - p(r,t)]}{141.2 \mu_i q_w}; \tag{3}$$

Reservoir mobility:

$$M = \frac{k_{fbi} / \mu_i}{k_{fbe} / \mu_e} \tag{4}$$

Diffusivity ratio:

$$\eta_D = \frac{k_{fbi} / \left[\phi_{fbi} c_{tfbi} + \phi_{mbi} c_{tmbi}\right]\ \mu_i}{k_{fbe} / \left[\phi_{fbe} c_{tfbe} + \phi_{mbe} c_{tmbe}\right]\ \mu_e} \tag{5}$$

Dimensionless conductivity of the fault:

$$F_{CD} = \frac{k_f w_f}{k_{fbi} d_f} \tag{6}$$

Skin fault factor :

$$S_f = \frac{2\pi k_{fbi}}{d_f}\left[\frac{w_a}{k_a} + \frac{w_f}{2k_f}\right] \tag{7}$$

Method of Solution

The solution is obtained by dividing the flow domain into the reservoir and the fault flow problems. These two flow problems are solved separately using the Laplace transform and coupled at the fault plane, by preserving continuity of pressure and flux from the two domains. This solution method is similar to the approach previously used to model pressure-transient behavior of finite-conductivity hydraulically fractured wells[23-26]. It is necessary that pressure-buildup data analyzed from a faulted reservoir, exhibit the effects of both fault conductivity and fault skin factor.

The Model

Because the fault thickness is very small, only linear flow inside the fault is considered. In addition, transient effects within the fault are assumed to end at early times and therefore are neglected. There are different types of flow in the reservoir from the left and the right hand side of the fault plane.

Radial flow in the reservoir

$$\frac{\partial^2 p_{fd}(r_D, t_D)}{\partial r_D^2} + \frac{1}{r_D}\frac{\partial p_{fD}(r_D, t_D)}{\partial r_D} + \frac{\pi}{F_{CD}}\frac{\partial\, p_{faD}(0, t_D)}{\partial x_D} = \frac{\partial\, p_{fD}(r_D, t_D)}{\partial t_D},$$

$$1 \le r_D < d_{fD} \tag{8}$$

Initial condition:

$$p_{fD}(r_D, 0) = 0 \tag{9}$$

Internal boundary at the wellbore: constant pressure

$$p_{fD}(1,t_D)=1 \quad (10)$$

Fault-reservoir boundary condition:

$$\frac{\partial p_{fD}(0,t_D)}{\partial z_D}=-\frac{\pi}{F_{CD}} \quad (11)$$

Linear transient flow within the fault:

$$\frac{\partial^2 p_{faD}(x_D,t_D)}{\partial x_D^2}+\frac{2}{F_{CD}}\frac{\partial p_{f1D}(1,t_D)}{\partial x_D}=\frac{1}{\eta_{faD}}\frac{\partial p_{faD}(x_D,t_D)}{\partial t_D}$$

$$0 \le x_D \le \infty \quad (12)$$

Initial Condition:

$$p_{fa}(x_D,0)=0 \quad (13)$$

Internal boundary:

$$p_{faD}(0,t_D)=p_{fD}(r_D,t_D) \quad (14)$$

External boundary:

$$\lim_{x_D\to\infty} p_{f1D}(x_D,t_D)=0 \quad (15)$$

Linear transient flow in the formation and perpendicular towards the fault plane.

$$\frac{\partial^2 p_{f1D}(y_D,t_D)}{\partial y_D^2}=\frac{1}{\eta_{f1D}}\frac{\partial p_{f1D}(y_D,t_D)}{\partial t_D};$$

$$d_{fD} \le y_D < \infty \quad (16)$$

Initial Condition:

$$p_{f1D}(y_D,0)=0 \quad (17)$$

Internal boundary:

$$p_{f1D}(d_{fD},t_D)=p_{faD}(x_D,t_D) \quad (18)$$

External boundary:

$$\lim_{y_D\to\infty} p_{f1D}(y_D,t_D)=0 \quad (19)$$

The pressure drop across the fault.

The reservoir and fault flow problems are coupled at the fault plane by preserving continuity of pressure and fluxes. An altered region around the fault is also considered during the coupling of the reservoir and fault solutions. The pressure drop across the fault and the associated altered zone (Fig. 3) are obtained by writing the Darcy equation and summing up all resistances to flow. The results obtained are:

$$p_{fD}(y_D,t_{Df})-p_{f1D}(y_D,t_{Df})=S_f\left[u_{fD}(y_D,t_{Df})-u_{f1D}(y_D,t_{Df})\right] \quad (20)$$

and

$$p_{fD}(y_D,t_{Df})-p_{f1D}(y_D,t_{Df})=S_f u_{f1D}(y_D,t_{Df}) \quad (21)$$

The solution to the problem of flow towards a well in the vicinity of a fault, given in terms of dimensionless flow rate in Laplace space is:

$$\overline{q}_D(s)=\frac{AI_1\left(\sqrt{sf(s)}\right)-BK_1\left(\sqrt{sf(s)}\right)}{sC} \quad (22)$$

where:

$$A=K_1\left(d_{fD}\sqrt{sf(s)}\right)-Ko\left(\sqrt{sf(s)}\right)/\pi\sqrt{sf(s)}$$

$$B=I_1\left(\sqrt{sf(s)}\right)/\pi\sqrt{sf(s)}+I_1\left(\sqrt{sf(s)}\right)$$

$$C=-I_1\left(\sqrt{sf(s)}\right)K_1\left(d_{fD}\sqrt{sf(s)}\right)+I_1\left(d_{fD}\sqrt{sf(s)}\right)K_1\left(\sqrt{sf(s)}\right) \quad (23)$$

$$f(s)=1+\frac{F_{CD}}{\pi s}\sqrt{\frac{2}{F_{CD}}\sqrt{\frac{s}{\eta_{f1D}}}+\frac{s}{\eta_{faD}}} \quad (24)$$

Although the skin is not explicitly considered in the model, it can be included by the convolution scheme in Laplace space[27].

A Laplace inversion algorithm, such as the Stehfest routine[28], was used to numerically invert Eq. 15, or its extension including a wellbore skin. An analysis should be performed to select the value of N, since for each solution in the Laplace space, there is a value of N that results in the correct numerical inversion toward real space, as compared with analytical solutions (in this case N was taken as 12).

Results

In the discussion to follow we first review the basic constant rate results of Abbaszadeh and Cinco[21], because of its close similarity to the constant pressure production decline behavior. Next we show results for the flow rate behavior of a well producing at constant pressure conditions, and the analysis of a field test of a well completed nearby a finite conductivity fault.

Effects of Fault Conductivity

Fig. 5 shows drawdown pressure and pressure-derivative type curves when the skin factor across the fault plane is equal to zero, and the reservoir properties on both sides of the fault are the same[21]. Wellbore storage and well skin effects are not included. Several curves as a function of conductivity of the fault plane, ranging from 10^{-1} to 10^{+8}, are shown on this figure. The derivative type curves start at the 0.5 level, which represents radial flow in the left hand-side reservoir.

Transparent fault

The curves deviate from the 0.5 level at t_{Df}=0.25 when pressure transients reach the fault plane. The degree of deviation depends on the conductivity of the fault plane. For conductivities less than 0.1, the pressure derivative stays on the 0.5 line, indicating that there is no flow along the fault plane and that fluid transfer occurs only across the fault.

This behavior is caused by the presence of very low conductivity that creates a large resistance to flow along the fault, while a zero *fault skin factor* would indicate no resistance to flow across the fault. Therefore, fluid flow is from the right hand-side reservoir to the left hand-side reservoir across the fault, as would occur if the fault plane would not exist.

A zero *fault skin factor* can occur when there is no altered region and either, the fault permeability is infinitely large or the fault plane is infinitely thin. The corresponding fault conductivities (Eq. 6) for these two limiting cases are $F_{CD} \to \infty$ as $k_f \to \infty$, and $F_{CD} \to 0$ as $w_f \to 0$, respectively; basically the latter condition would mean that the fault would not exist. Thus, a fault with a zero *fault skin factor* and a small conductivity results from a very thin fault plane with an unaltered region around it. Such a fault system will not have any conductivity for flow to occur along it.

Dominant fault

For high-conductivity cases, the fault plane initially acts as a linear constant-pressure boundary[13] on a pressure derivative plot (a straight line with a negative unit slope). As time progresses, pressure at the fault plane decreases, causing fluid entering the fault linearly from the reservoir, flowing linearly along it, and exiting from the fault plane towards the producing well. This flow characteristic is seen as a bilinear flow on a pressure derivative plot (a straight line with a quarter slope)[23]. At later times, when transients practically have passed the fault system, the behavior reflects the entire reservoir response, and the derivative curves again reach asymptotically the 0.5 line (note that the mobility ratio for this example is unity).

It is interesting to note that the pressure-transient behavior for intermediate values of fault conductivity is similar to that exhibited by NFR. The presence of a single conductive fault in a homogeneous reservoir can give the appearance of a naturally fractured reservoir on pressure-transient tests[13]. However the quarter-slope straight-line bilinear flow signature, is not developed on transient-pressure responses. This is in contrast to pressure-transient behavior of *finite conductivity* fractured wells, where both pressure and pressure derivative exhibit quarter-slope straight lines parallel to each other.[23]

The absence of the bilinear flow signature on pressure responses is attributed to the existence of pseudoskin, due to an incompressible flow region around the well at the time when the effect to the fault is sensed at the wellbore.

The wellbore pressure for the bilinear flow regime when there is a contrast in reservoir mobilities at both sides of the fault is:[27]

$$p_{wD}(t_{Df}) = \frac{2.45}{\sqrt{2F_{CD}\left[\sqrt{M}+1\right]/\sqrt{M}}} t_{Df}^{1/4} + C_1 \qquad (25)$$

and the pressure derivative group:

$$t_{Df}\frac{dp_{wD}(t_{Df})}{dt_{Df}} = \frac{0.8622}{\sqrt{F_{CD}\left[\sqrt{M}+1\right]/\sqrt{M}}} t_{Df}^{1/4} \qquad (26)$$

Eq. 7 indicates that a plot of pressure vs. the fourth root of time is a straight line with a slope related to conductivity and mobility ratio. This bilinear behavior has been observed previously in field tests[1]. A comparison of Eqs. 25 and 26 with the finite-conductivity fractured well solutions [30, 31] indicate that the fault system behaves as a fractured well with effective conductivity equal to $2F_{CD}\left[\sqrt{M}+1\right]/\sqrt{M}$, and the fracture having a flow restriction in the vicinity of the wellbore.

For low conductivity values (e.g., F_{CD}= 0.01), the fluid transfer is only across the fault because fluxes from both the right hand- and the left hand-side reservoirs are essentially identical having opposite signs.

For high conductivity values, there is very little contribution to flow from the right hand-side reservoir and the drainage is primarily from the left hand-side reservoir domain through the fault plane. Therefore, the fault acts as a source of fluid supply.

Effects of Fault Skin Factor[21]

Fig. 7 shows pressure derivative type curves in the presence of fault skin factor. Reservoir properties are the same everywhere. The effect of skin factor at the fault plane is to create additional resistance to flow across for some period of time, resembling a situation similar to a sealing fault for all conductivity values.

Pressure derivatives after the onset of the fault effects tend to approach the behavior of doubling of the semi-log straight line slope[3-6] (pressure derivative groups equal to 1), for S_f >100.

At larger times, when pressure on the left hand side of the fault becomes low enough to allow for appreciable flow to cross the fault plane, pressure transients propagate through the right hand-side reservoir, and the behavior becomes similar to the S_f = 0 case. The negative-unit-slope straight line of a constant-pressure linear boundary, and the quarter-slope line of bilinear flow characteristics, are both developed for high conductivity values, and eventually, derivative curves approach the 0.5 level (combined reservoir behavior).

A general equation for the constant-pressure linear-boundary-dominated region was presented by Yaxeley[15]. The pressure derivative function from this equation shows a negative-unit-slope line behavior on a Log-Log plot, given by[27]:

$$t_{Df}\,\frac{dp_{wD}(t_{Df})}{dt_{Df}} = \frac{1}{2}\left[\,1+\frac{S_f^{\,2}}{2\pi^2}\,\right]\,t_{Df}^{\,-1} \qquad (27)$$

Previous works[15,16,17] have modeled a fault system either as a skin zone, or as a partially communicating barrier. These cases correpond to the zero conductivity cases in **Fig. 7** (the behavior above the 0.5 level). The behavior for F_{CD}>0 (below the 0.5 level) is entirely a result of flow along the fault, which is characterized by the conductivity factor.

A semilog plot of dimensionless pressure for cases of fault skin factor of S_f = 0 and S_f = 1,000 is shown in **Fig. 8**. This figure illustrates that there is a single straight line with a slope of 1.151 at all times for S_f = 0 and F_{CD}<0.1.

As the conductivity of the fault increases, the pressure response deviates from this straight line, following another line parallel to the first straight line. This behavior is similar to the typical pressure-transient response from NFR. Pressure is essentially flat within the testing period for very large conductivity values, indicating constant-pressure boundary effects.

For S_f = 1,000 and low values of fault conductivity, there is an initial straight line with a slope equal to 1.151, representing the response from the left hand-side reservoir. Next, doubling of the slope occurs, indicating sealing fault behavior. Finally, a third straight line parallel to the initial straight line with a slope equal to 1.151 develops, which represents the combined response from the entire reservoir. If the reservoir mobility ratio is different from unity, the slope of the third straight line would be 2.303M/(1+M) for $\eta_D = 1$, as previously shown by Bixel *et al.*[16]

Effect of Mobility and Diffusivity Contrast[21]

When properties of the reservoir at two sides of a fault plane are not the same, complexities in addition to fault conductivity and skin effects are introduced. The effect of mobility ratio is more pronounced for the low-fault-conductivity cases. For large conductivity values, because

fluid may enter the fault and simply travel along the fault plane, the pressure derivative tends to follow the constant-pressure linear boundary characteristic of the negative-unit-slope line for all conductivity values, and eventually reaches a level equal to *M/(1+M)*. Also, as the mobility ratio approaches zero, the right hand-side reservoir acts like a pressure support and becomes indistinguishable from a conductive fault. For this case, pressure derivatives follow a negative-unit-slope line for all conductivity values. The contrast in storativity does not significantly alter the transient pressure responses.

Field Example

A 24 hours pressure-buildup test was carried out in a well completed in a heavily faulted naturally fractured reservoir, located nearby a conductive fault; Fig. 9 shows a log-log flow diagnosis graph, showing that at early times, t < 0.8 hr, wellbore storage dominated the pressure response. For later times basically the pressure behavior follows a half slope, which is characteristic of the formation flow period present in hydraulically fractured wells; geological and geophysical information indicate the presence of a fault in the vicinity of the well, the best distance estimation being about 20 m. It should be pointed out that due to the close distance of the fault from the well, the pressure response shown by this well is similar to the case where the well is intercepted by a fault.

Based on the previous results of the diagnosis of flow regimes, Fig.10 shows a Cartesian linear graph of the data registered during this test; the estimation for the fault permeability was 156 md (the slope of the graph was 170 psi/hr$^{1/2}$).

Constant Pressure Production Decline Behavior.

The Laplace space solution given by Eqs. 22 to 24 was inverted through the procedure already discussed, for values of the fault skin factor, $s_f = 0$, dimensionless fault conductivity, $F_{cD} = 200$, diffusivity ratio, $\eta_D = 500$ and reservoir mobility ratio, $M = 1$, distance to the fault of 20 m Fig.11; this distance was chosen based on the field results of the last section.

Results of this figure show an early linear flow behavior which is caused by the short distance from the fault to the well, which results in a similar behavior as if the fault were to intersect the well; next a transition period is followed, and finally bilinear flow is reached, which is due to the combination of the linear flow from the reservoir to the fault and linear flow in the fracture.

Fig. 12 shows additional dimensionless results of the flow rate vs. time graphed also in log-log scale, for values of the fault conductivity F_{CD} of 2 and 5, and for three different values of the diffusivity ratio, 0.1, 1 and 10; basically these results present the same characteristics already discussed for the flow behavior exhibited in Fig.11.

<u>Production forecast analysis</u>

From an engineering and economic point of view, the initial decline could be a key factor in the completion or abandonment of a well.

Decisions concerning production forecasts and estimates of the size of fractured reservoirs should not be based only on the observed initial decline. Ignoring the presence of a conductive fault plane in a NFR can lead to a great error on the estimation of the cumulative production.

The results show that the initial decline could be a key factor in deciding whether to change or abandon a well, and for a practical viewpoint, given an initial value for the flow rate, it is important to know the time required to deplete the dual porosity system with a conductive fault system.

An expression for the flow rate can be derived from the dimensionless wellbore pressure function for constant rate production after the onset of pseudo steady state. van Everdingen and Hurst[32] showed that knowing the pressure in the well, it is possible to find the flow rate by applying the inverse Laplace transformation to the following relationship:

$$1 = \int^{t_D} q_D(t_D - \tau_D) \frac{dp_{wD}(\tau_D)}{d\tau_D} d\tau_D \quad (28)$$

Applying the Laplace transform:

$$\frac{1}{s} = \overline{q_D(s)} \bullet s\,\overline{p_{wD}(s)} \tag{29}$$

Solving the dimensionless flow rate;

$$\overline{q_D(s)} = \frac{1}{s^2\,\overline{p_{wD}}(s)} \tag{30}$$

For bilinear flow conditions, the dimensionless pressure has been expressed as:

$$p_{wD}(t_D) = \frac{2.45}{\sqrt{F_{CD}}} t_{Ddf}^{1/4} \tag{31}$$

Applying the Laplace transform to eq. 27:

$$\overline{p_{wD}(s)} = \frac{\pi}{\sqrt{2F_{CD}}} \frac{1}{s^{5/4}} \tag{32}$$

Substituting eq. 31 in eq. 30:

$$\overline{q_D(s)} = \frac{1}{s^2\left[\pi / \sqrt{2F_{CD}}\right] s^{-5/4}} = \frac{\sqrt{2F_{CD}}}{\pi s^{3/4}} \tag{33}$$

The analytical inversion is given by:

$$q_D(t_{Ddf}) = \frac{\sqrt{F_{CD}}}{2.45\,\Gamma(3/4)} t_{Ddf}^{-1/4} \tag{34}$$

Eq. 33 indicates that a Cartesian graph in terms of dimensionless variables, of $1/q_D$ vs $t_{Ddf}^{1/4}$ will show a linear behavior, corresponding to bilinear flow, that would prevail whenever most of the produced fluid comes from the formation, and fault tips effects have not yet affected the well behavior (it should be kept in mind that the model of the present work considers the fault to be of infinite length).

Conclusions

1. An analytical solution is developed that describes decline curve analysis in a NFR for a well near a nonintersecting finite-conductivity fault of infinite length. The solution considers both flow across and within the fault along the fault plane. An altered region around the fault is included, and reservoir properties are allowed to be different on two sides of the fault.
2. Type curves of flow rate as a function of the fault parameters of conductivity and skin factor, and the reservoir parameter of conductivity ratios are developed. The parameter of distance to the fault is considered in the definition of dimensionless time.
3. For large fault skin factors, transient behavior initially resembles a sealing fault for all conductivities, until sufficient flow communication across the fault plane is established.
4. Pressure derivative type curves eventually become horizontal at a level related to reservoir mobility ratios. This behavior could be similar to that of naturally fractured reservoirs for the unit-mobility-ratio case. Thus, a single conductive fault can give an appearance of a naturally fractured reservoir on a pressure-transient response.

Nomenclature

B = formation volume factor, RB/STB.
C = wellbore storage, bbl/psi.
c_t = total compressibility, Lt^2/m, psi^{-1}
d_f = distance of fault plane located from an active well, L, ft.
Ei = exponential integral.
F_{CD} = conductivity of fault plane, dimensionless.
F_s = storativity ratio $(\phi c_t)i/(\phi c_t)_e$.
h = reservoir thickness, L, md.
k = reservoir permeability, L^2, md.
k_a = altered permeability around fault, L^2, md.
k_f = permeability of fault plane, L^2, md.
K_0 = Bessel function of the first kind.
L_f = fault length, L, ft.
M = mobility ratio, dimensionless.
p = pressure, m/Lt^2, psi.
p_f = pressure in the fault plane, m/Lt^2, psi.
p_i = initial reservoir pressure, m/Lt^2, psi.
p_w = wellbore pressure, m/Lt^2, psi.
U_{fl} = flux from left-side reservoir into fault, L, ft.
U_{fl} = flux from right-side reservoir into fault, L, ft.
u_f = net flux to/from fault, L, ft.
q_w = constant drawdown rate of active well, L^3/t, STB / D.
r_w = wellbore radius, L, ft.

S_w = skin around wellbore, dimensionless.
S_f = skin fault, dimensionless.
s = Laplace transform parameter.
t = time, t, hr.
w_a = extent of altered zone around the fault, L.
w_f = width of fault plane, L, ft.
x = coordinate normal to fault, L, ft.
y = coordinate parallel to fault, L, ft.
y' = integration variable.
ϕ = porosity, fraction.
μ = viscosity, m/Lt, cp.
τ = time integration variable.
$\eta = \frac{k}{\phi \mu c_t}$ = diffusivity, L^2/t, ft^2/hr.
η_D = diffusivity ratio, dimensionless.

Subscripts

b = bulk (matrix and fractures).
D = dimensionless.
i = region containing active well (left-side).
e = region not containing active well (right side).
f = fracture

ACKNOWLEDGMENTS

Our appreciation to Eng. Guadalupe Galicia for her careful and constructive reviews. Discussions with M.Sc. Geophysicist Arturo Castro were invaluable. Special thanks to Eng. Ricardo Martínez and the late Geologist Cesar Rosas for their comments. Portion of this study were done by Héctor Pulido as PhD. graduate degree requirements Financial support was provided by PEMEX and UNAM.

References

1. Trocchio, J. J. (1990): ***Investigation of Fateh Mishrif Fluid Conductive Faults,*** JPT (Aug.) 1038; Trans., AIME, 289.
2. Smith, D. A.(1966): ***Theoretical Considerations of Sealing and Nonsealing Faults***, AAPG Bull (Feb.) **50**, No.2, 363-374.
3. Horner, D. R. (1951): ***Pressure Buildup in Wells***, Proc., Third World Pet. Cong., The Hague Sec. **II**, 503-23.
4. Stallman, R. W.(1952): ***Nonequilibrium Type Curves Modified for Two-Well Systems***, Geol. Survey Groundwater, Note 3, U. S. Dept. of Interior, Washington.
5. Davis, E. G. and Hawkins, M. F. (1963): ***Linear Fluid-Barrier Detection by Well Pressure Measurement***, *JPT* (Oct.) 1077.
6. Gray, K. E. (1965): ***Approximating Well-to-Fault Distance from Pressure Buildup Test***, *JPT* (July) 761.
7. Earlougher, R. C. and Kazemi, H. (1980): ***Practicalities of Detecting Faults from Buildup Testing***, *JPT* (Jan.) 18.
8. Prasad, R. K. (1975): ***Pressure Transient Analysis in the Presence of Two Intersecting Boundaries***, JPT (Jan.) 89; *Trans*., AIME, **259**.
9. Tiab, D. and Kumar, A. (1980): ***Detection and Location of Two Parallel Sealing Faults Around a Well***, JPT (Oct.) 1701.
10. Earlougher, R. C. Jr. (1968): ***Pressure Distributions in a Rectangular Reservoirs***, *JPT* (Feb.) 199. *Trans*., AIME, **243**.
11. Ehlig-Economides, C. and Economides, M. J. (1985): ***Pressure Transient Analysis in an Elongated Linear Flow Systems***, SPEJ (Dec.) 839.
12. Streltsova, T. D. and McKinley R. M.: ***Effect of Flow Time Duration on Buildup Pattern for Reservoirs with Heterogeneous Properties***, SPEJ (June 1984) 294.
13. Cinco-Ley, H., Samaniego, F. V. and Domínguez, A. N.(1976): ***Unsteady State Flow Behavior for a Well Near a Natural Fracture***, paper SPE 6019 presented at the SPE Annual technical Conference and Exhibition, New Orleans, Oct. 3-6.
14. Stewart, G., Gupta, A., and Westaway, P. (1984): ***The Interpretation of Interference Tests in a Reservoir With a Sealing and a Partially Communicating Faults***, paper SPE 12967 presented at the SPE European Offshore Petroleum Conference, London, Oct. 25-28.
15. Yaxeley, L. M. (1987): ***Effect of Partially Communicating Fault on Transient Pressure Behavior***, SPEFE (Dec.) 590; Trans., AIME, **283**.
16. Bixel, H. C., Larkin, B. K., and Van Poolen, H. K.(1963): ***Effects of Linear Discontinuities on Pressure Buildup and***

Drawdown Behavior, *JPT* (Aug.) 885; *Trans*., AIME, **228**.

17. Ambastha, A. K., McLeroy, P. G., and Grader, A. S. (1989): ***Effects of Partially Communicating Fault in a Composite Reservoir on Transient Pressure Testing***, SPEFE (June) 210.
18. van Everdingen, A. F. (1953): ***The Skin Effect and its Influence on the Productivity Capacity of a Well,*** *JPT* (June) 171; *Trans*., AIME, **198**.
19. Hurst, W. (1953): ***Establishment of the Skin Effect and Its Impedement To Fluid Flow in a Wellbore,*** *Pet. Eng*. (Oct) B6-B16.
20. Khachatoorian, R., Ershaghi, I. and Shikari, Y. (1995): ***Complexities in the Analysis of Pressure transient Response in Faulted Naturally Fractured Reservoirs,*** SPE Formation Evaluation J. (September).
21. Abbaszadeh, M. D. and Cinco-Ley, H. (1995): ***Pressure Transient Behavior in a Reservoir with a Finite-Conductivity Fault,*** SPE Formation Evaluation (March) 26-32.
22. Earlougher, R. C. jr. (1977):***Advances in Well Test Analysis,*** *Monograph Series*, SPE, Richardson, TX **5**.
23. Cinco-Ley, H. and Samaniego, F. V. (1981): ***Transient Pressure Analysis for Fractured Wells***, *JPT* (Sept.) 1749.
24. Guppy, K. H., Cinco-Ley, H., and Ramey, H. J. (1981): ***Effect of Non-Darcy Flow on the Constant-Pressure Production of Fractured Wells,*** SPEJ (June) 390.
25. Guppy, K. H. Cinco-Ley, H., and Ramey, H. J. (1982): ***Non-Darcy Flow in Wells with Finite-Conductivity Vertical Fractures***, *SPEJ* (Oct.) 681.
26. Cinco-Ley, H. and Meng, H. Z. (1988): ***Pressure-Transient Analysis of Wells with Finite-Conductivity Vertical Fractures in Double Porosity Reservoirs***, Paper SPE 18172 presented at the SPE Annual Technical Conference and Exhibition, Houston, Oct. 2-5.
27. Abbaszadeh, M. D. and Cinco-Ley, H. (1988): ***Supplement to SPE 24704, Pressure Transient Behavior in a Reservoir with a Finite-Conductivity Fault,*** Paper 30227 available at SPE, Richardson, TX.
28. Stehfest, H. (1970): ***Algorithm 368, Numerical Inversion of Laplace Transforms,*** *Communications of the ACM* (Jan.) **13**, 47-49.
29. Agarwal, R. G., Al-Hussainy, R., and Ramey, H. J. Jr. 1970): ***An Investigation of Wellbore Storage and Skin Effects in Unsteady Liquid Flow: I. Analytical Treatment***, *SPEJ* (Sept.) 270; *Trans*., AIME **249**.
30. Cinco-Ley, H. and Samaniego, F. V. (1981): ***Transient Pressure Analysis: Finite Conductivity Fracture Case Vs. Damaged Fracture Case***, paper SPE 10179 presented at the SPE Annual Technical Conference and Exhibition, San Antonio, Oct. 5-7.

Wong, D. W., Harrington, A. G. and Cinco-Ley, H. (1986): ***Aplication of the Pressure Derivative Function in the Pressure Transient Testing of Fractured Wells***, SPEFE (Oct. 1986) 470; Trans., AIME, 281.

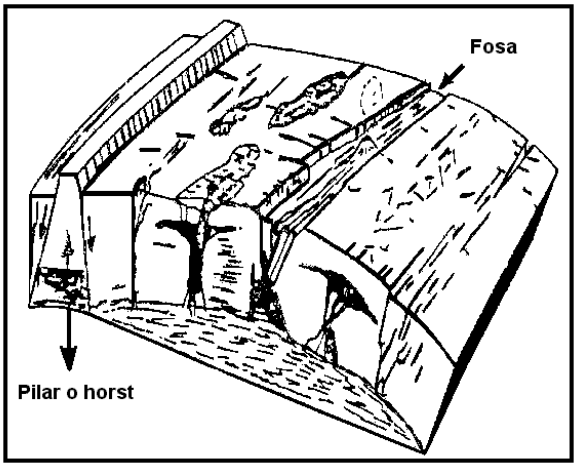

Fig. 1. Visualization of a real faulted reservoir.

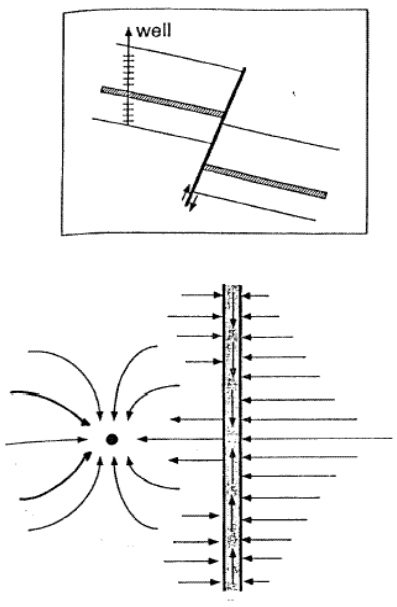

Fig. 2 schematic of a typical fault system and flow lines[21].

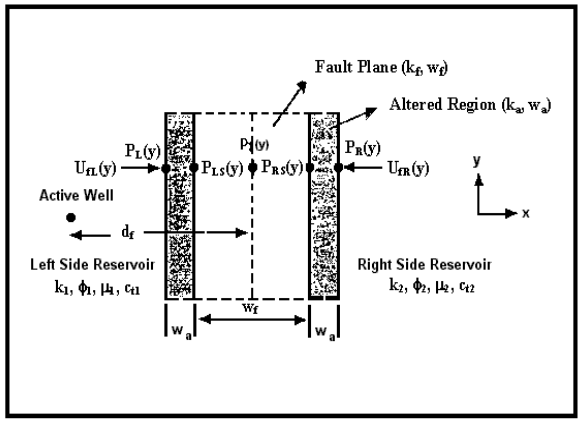

Fig. 3. Schematic of restrictions a the Fault Plane model associated with a nomenclature.

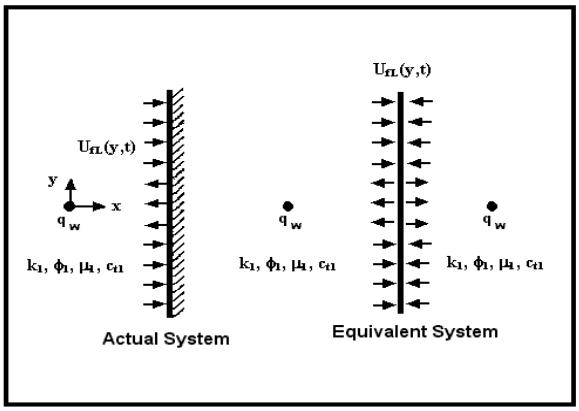

Fig. 4. Image of the left side of the fault, using radial flow.

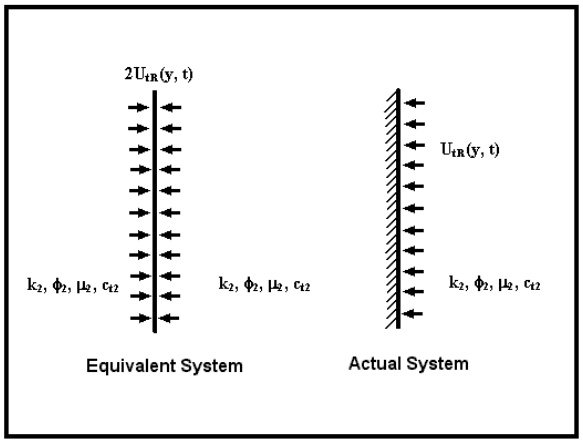

Fig. 5. Image of the right side of the fault, using linear flow.

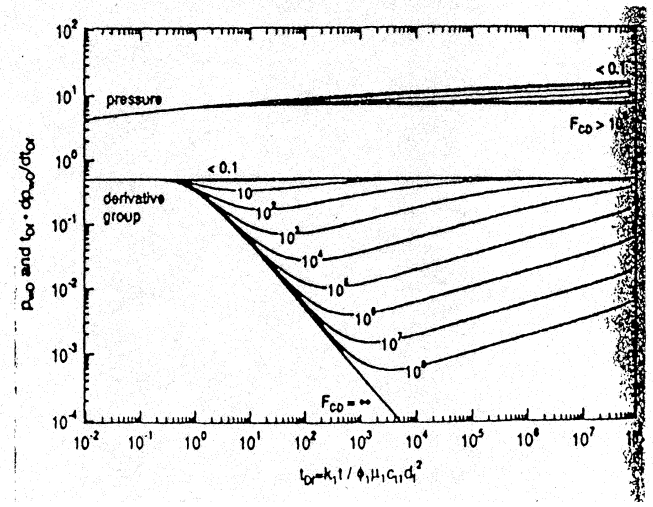

Fig. 6. Generalized derivative type curves for a finite conductivity fault, for S_f=, M=1, $\eta_D = 1$.

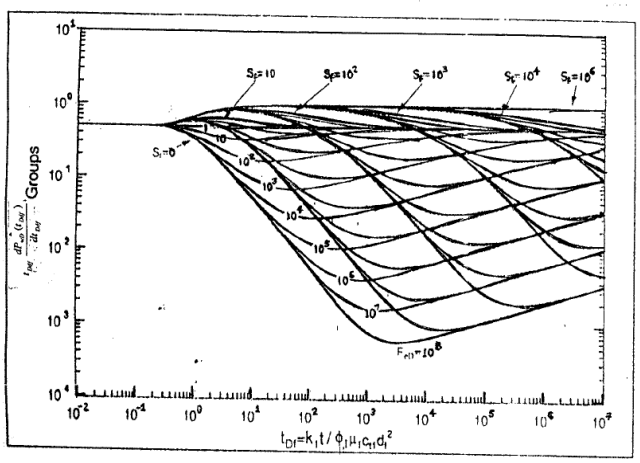

Fig. 7. Generalized derivative type curves for a finite conductivity fault, for different skin fault factor, M=1, $\eta_D = 1$.

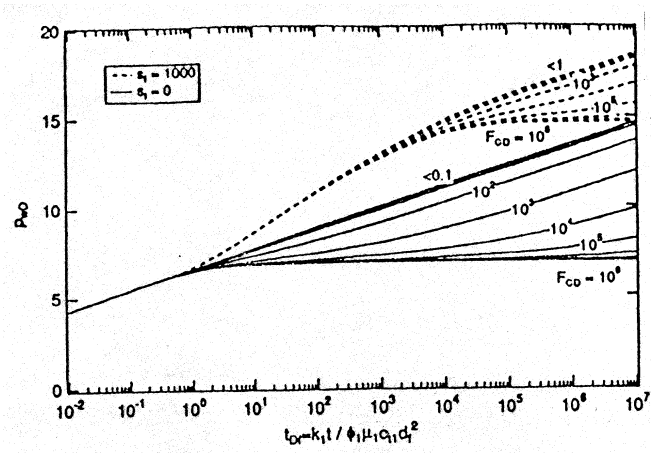

Fig. 8. Semilog plot of pressure response for two values of fault skin factor, M=1, $\eta_D = 1$.

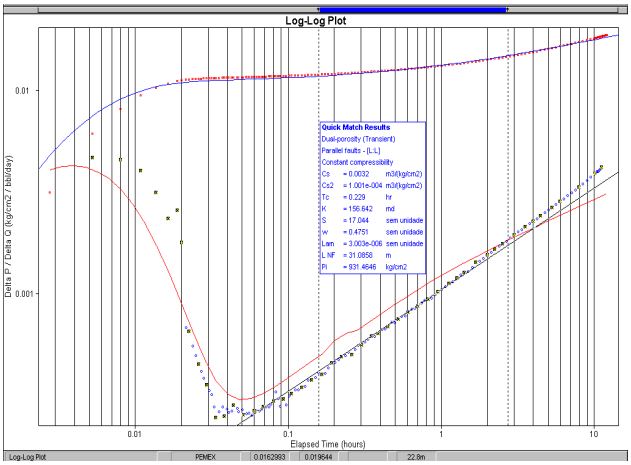

Fig. 9. Detecction of the dominant faul near a well generating linear flow.

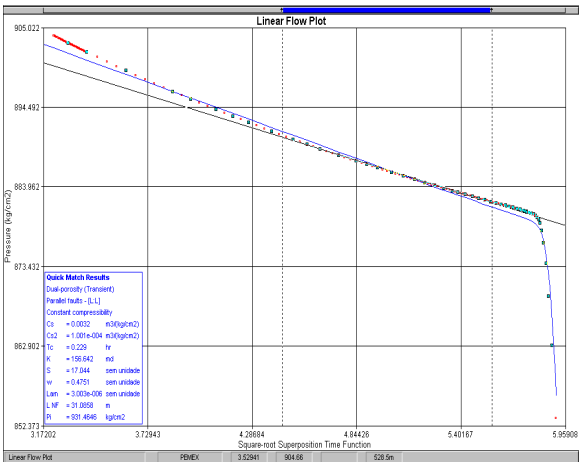

Fig. 10. Using specialized graphs for interpretations.

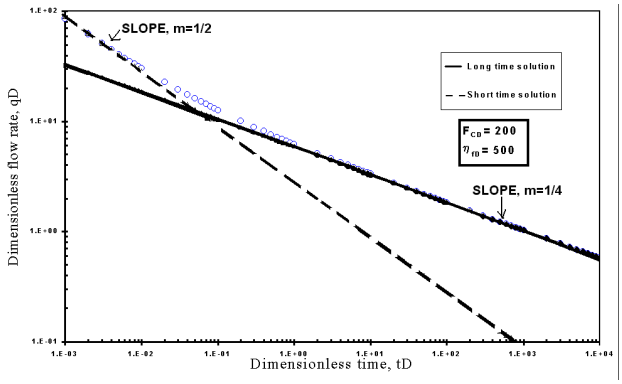

Fig. 11. Transient dimensionless flow rate of a well producing under constant pressure conditions, near a finite conductive fault, compared with approximate analytical solution for long and short times, M=1.

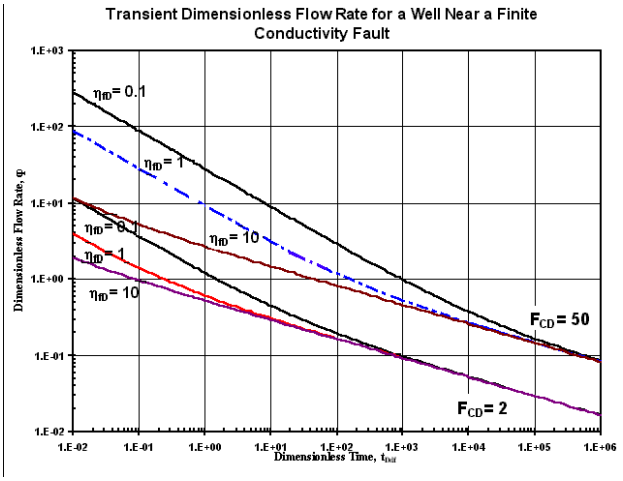

Fig. 12. Transient dimensionless flow rate of a well producing under constant pressure conditions, near a finite conductive fault, for different conductivities and diffusivities.